Scientific Research Publishing

Economic Geology Study with Focus on Cu Mineralization (Fath Abad Area, Khorasan Razavi)

Reza Ehsani, Naghmeh Mohamadi, Mohamd Hossain Ehsani

Geology Department, Islamic Azad University of Tehran, North Branch, Tehran, Iran

Email: Rezaehsani@live.com

Abstract

The study area is located in south of Khorasan-Razavi province. This region is part of central Iran, which is of high significance due to existence of metal and non-metal deposits. Considering the location of the study area, the lithology and metal-mineral indices of Dolat-Abad sheet, it can be said that their metallic deposits are economically feasible. Hence, this region is considered promising for exploration of metallic deposits. In order to achieve this goal, at first, the region's alterations were detected by using OLI-ASTER images in ENVI software. After processing the lithogeochemical data in SPSS and GIS software, anomaly map of studied elements was obtained. Using geological map, different layers such as lithology, faults and indices were obtained. Eventually, by preparing the layers and incorporating those using the index overlay GIS modeling, promising mineralization areas in the region were identified. Results show that a significant Cu-Au mineralization has occurred in the south western region of the study area.

Keywords

1. Introduction

The study area is located in the southern region of Khorasan Razavi province, in eastern Rashtkhar, a subordinate of Torbat Heydarieh. The study area's coordinate on the UTM visual system (zone 40) is between 755117 and 760614 Longitude and 3882437 and 3879927 Latitude and is located in 1:250000 geological map of Torbat Heydarieh and 1:100000 sheet of Dolat-Abad [1]. The study area has complex fault displacements and fractures. Movement effects, magma replacements and the eruption of lava are among the controlling factors of mineral deposition conditions of the area. The inter-fracture and plurality of the tectonic activities within phenomena such as swirling,

shearing, and probably vertical movements of the blocks has caused the formation of the reverse, normal and crossover system faults, and the transformations caused by them have led to necessary conditions for the intrusion or eruption of magma. In addition, the contact and regional metamorphosis has also occurred in the region. The Doruneh fault is one of the most significant faults of the study area, located in south of the region, with north-northeast to south-southwest trend and stretching for about 38 km. This fault's dip is more than 35 degrees to the northwest and it is considered as a reverse fault. This fault is responsible for moving the northeastern deposits towards the southwest [2] [3].

There are also faults in the central region, most of which are in line with the Doruneh fault. In addition, there are crossover systems which have made Eocene volcanic eruptions possible. In the northeastern part of the region, a number of reverse faults can be seen, most of which are in line with Doruneh fault, but their dip is towards southwest and has slid the Cretaceous deposits over the precambrian metamorphic rocks. In northwest of the study area, a succession of an ophiolite suite is outcropped and hosted by the fault's adjacent rocks. These faults are mainly in line with the Doruneh faults, and crossover systems can also be seen among them. In terms of economic geology, lens-shaped deposits of manganese and ferrous ores with a cauliflower and striped texture are exposed in the region. In the east of the study area and upper section of the Eocene tuffs, a layer of relatively high grade gypsum with sedimentary-evaporative origin is outcropped. Siliceous outcrop in Triassic units can be seen on the way to Zharf and Sultan Soleyman villages in northeast of the study area. These outcrops are not very big in size but they are high grade. With regard to the origin of the silicic veins and blocks, it is believed that silicium oxide have penetrated sedimentary deposits in different ways, and the subsequent pressure has caused these silicium bearing fluids to move, which has caused the deposition of silicium oxide in proper locations in different forms. The study area has a complex geological structure which has made it suitable for the formation of different mineral deposits.

2. Remote Sensing Studies

2.1. Alteration Detection in the Study Area with the Operational Land Imager (OLI) Sensor

To detect alteration groups in the area, various techniques such as False Color Composite (FCC)), Crosta principal component analyses (PCA), least squares regression fit (LS-Fit) and Spectral Angle Mapper (SAM method) were conducted on the images.

2.1.1. False Color Composite Method (FCC)
Figure 1 shows the true color composite of the study area using (RGB 3, 2, 1) bands. Figure 2 shows False Color Composite using (RGB 5, 3, 1). This band spectrum is suitable for revealing the topography of the study area.

2.1.2. Principal Components Analysis (PCA)
The principal component transformation is a multivariate statistical technique that selects uncorrelated linear combinations (eigenvector loadings) of variables in such a way
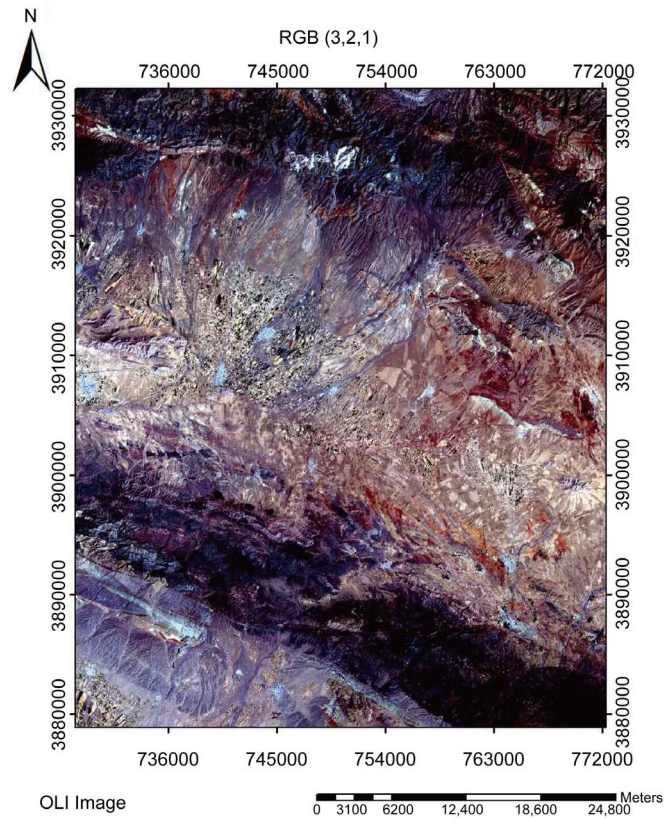
Figure 1. True color composite.
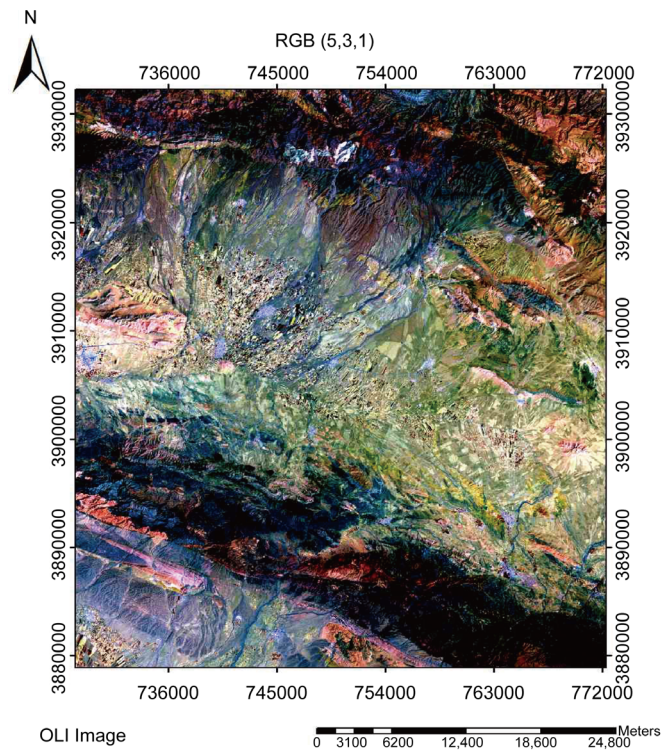
Figure 2. False color composite.

that each successively extracted linear combination, or principal component, has a smaller variance. The statistical Variance in multispectral images is related to the spectral response of various surficial materials such as rocks, soils, and vegetation, this method was used to generate uncorrelated output bands and separate noise components and reduce output data volume. Three different methods of principal component analysis including standard principal components analysis, Principal components analysis with Crosta method and selective Principal components analysis (SPCA) were conducted. The following are the results of each method [4].

1) Principal Components Analysis Using the Crosta Technique

In this method, Principal component analysis is usually conducted on bands (5,1,3,4) to detect areas containing Iron oxide, and conducted on bands (7,1,4,5) to reveal areas containing hydroxyl minerals. The Eigenvalue matrix of the Crosta method is shown in Table 1 and Table 2, according to which, considering the existing maximum differences between bands 5 and 7 in the fourth row of Table 1, PC4 is used to detect areas with hydroxyl mineral concentration, and considering the negative eigenvalue of band 5, in order to show areas containing Clay minerals in bright pixels, PC4 needs to be negated (Figure 3). Also considering the maximum value difference between bands 3 and 1 in the fourth row of Table 2, PC4 is suitable for detecting areas containing iron oxide (Figure 4).

2) Least Squares Regression Fit (LS-Fit)

Due to the high reflection rate of hydroxyl minerals in Band 5 from OLI satellite images, this band was used to detect argillic alterations (Figure 5) and because of the high reflection rate of iron oxide in band 3, this band was used to detect iron oxide alteration (Figure 6).

2.2. Detection of Alterations in the Study Area Using ASTER Images

In order to detect alterations in the study area, different techniques were conducted on the images.

Table 1. Eigenvalues of Bands 1,4,5,7.

Eigenvector	Band 1	Band 4	Band 5	Band 7
PC1	0.183992	0.533982	0.590189	0.57679
PC2	0.076231	−0.823178	0.211461	0.521394
PC3	−0.945028	−0.015232	0.326130	−0.018148
PC4	−0.259341	0.192378	−0.707531	0.62859

Table 2. Eigenvalues of Bands 1,3,4,5.

Eigenvector	Band 1	Band 3	Band 4	Band 5
PC1	−0.201659	−0.481106	−0.586749	−0.619351
PC2	−0.300341	−0.387659	−0.795889	−0.355073
PC3	−0.457129	−0.543318	−0.128247	0.692381
PC4	−0.812504	0.568386	−0.076417	−0.104574
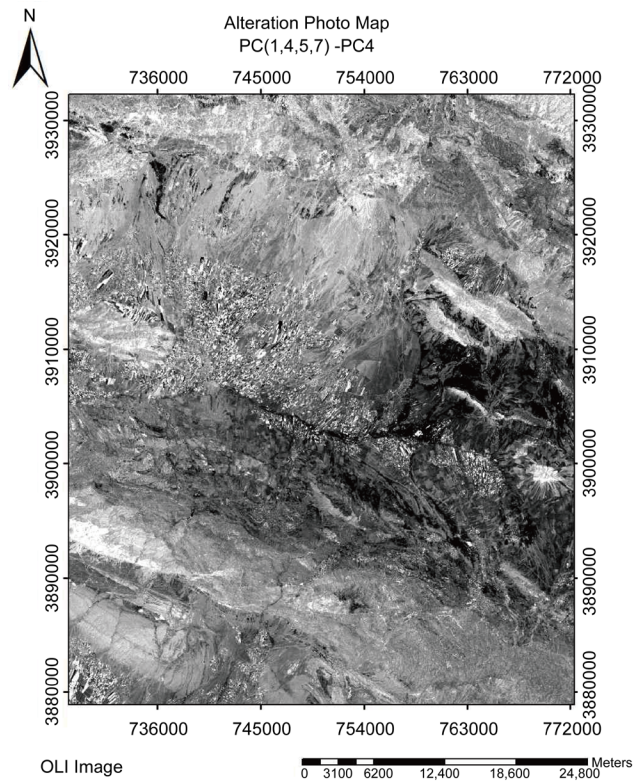
Figure 3. Bright pixels are indicative of argillic alteration.
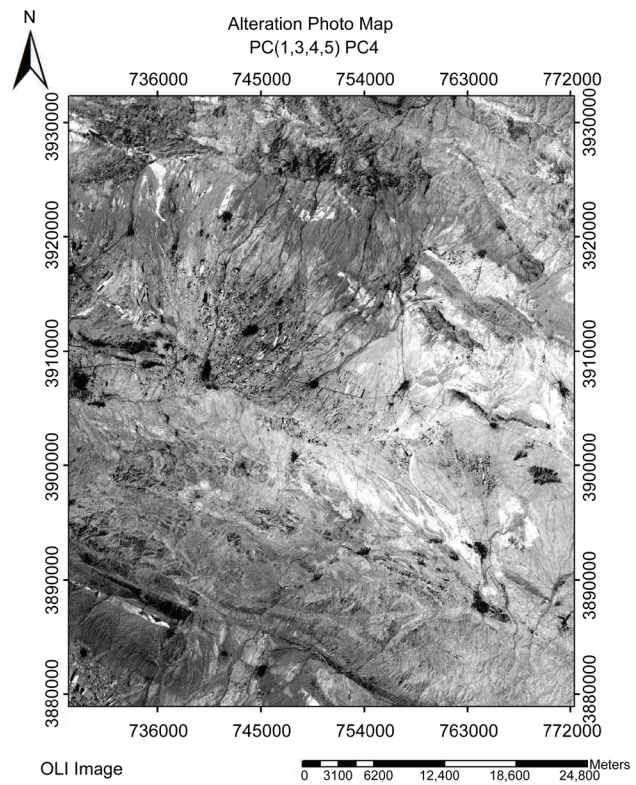
Figure 4. Bright pixels are indicative of iron oxide.
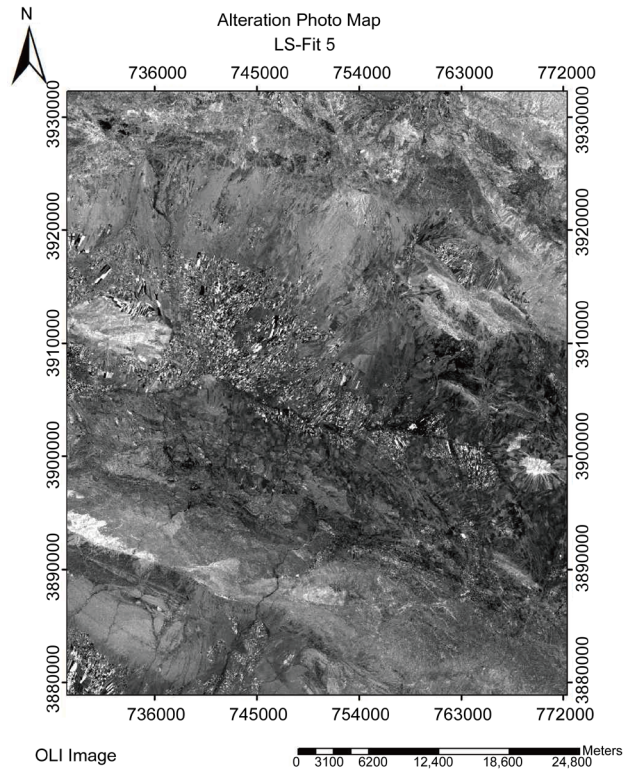
Figure 5. Bright pixels are indicative of argillic alteration.
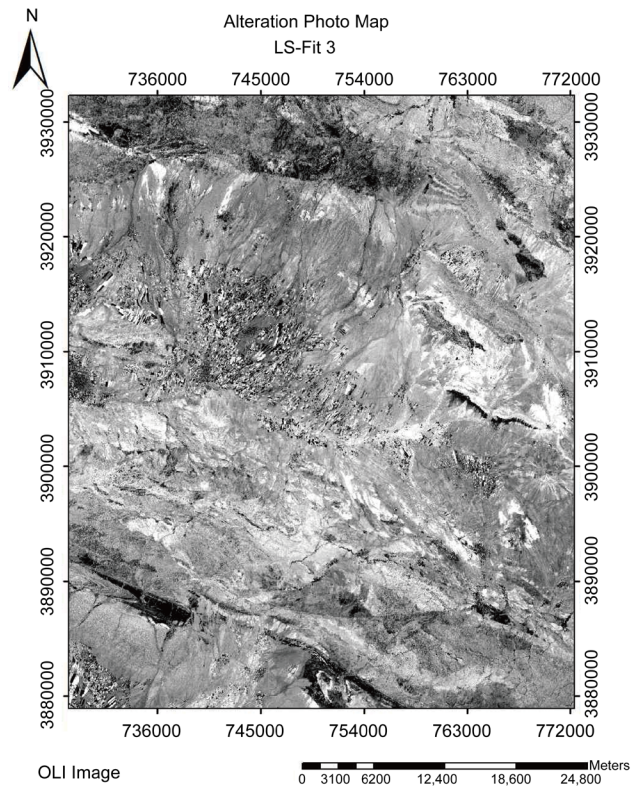
Figure 6. Bright pixels are indicative of iron oxide.

2.2.1. False Color Composite Method (FCC)

One of the most efficient band composites used in distinguishing alteration in ASTER images is the band composite of RGB4, 6, and 8. In this color composite, the argillic alterations are identified with pink, propylitic alterations are identified with green and areas containing lime are identified with yellow colors (**Figure 7**).

2.2.2. Principal Components Analysis Using the Crosta Technique on ASTER Images

Considering the spectral characteristics of montmorillonite, kaolinite, illite and muscovite, (indicatives of argillic and phyllic alteration zone) and minerals such as chlorite and epidote (indicators of propylitic alterations zone), preferred bands were selected for principal component analysis. Then, according to the characteristics of the index minerals of desired alterations, Principal components (1,2,3,4), (4,6,7,9), (1,4,6,7) and (2,5,8,9) were used to detect iron oxide, argillic alteration, phyllic alteration and propylitic alteration respectively. According to eigenvalues tables and the spectral behavior of index bands of each of the studied alterations, the fourth component in **Table 3**, the third component in **Table 4**, the fourth component in **Table 5** and the negative value of
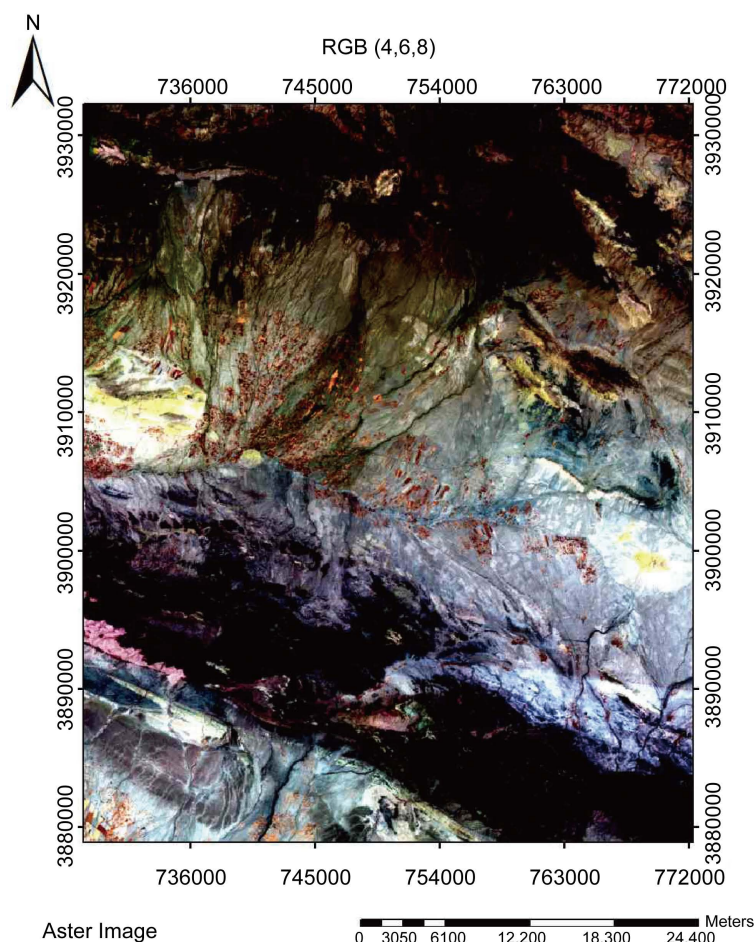
Figure 7. False color composite (RGB 4,6,8).

Table 3. Eigenvalues of bands 1,2,3,4.

Eigenvector	Band 1	Band 2	Band 3	Band 4
PC1	−0.420730	−0.522777	−0.495366	−0.551637
PC2	−0.423357	−0.416080	−0.091675	0.799526
PC3	0.389194	0.247313	−0.855174	0.236730
PC4	−0.701629	0.701725	−0.122005	−0.020325

Table 4. Eigenvalues of bands 4,6,7,9.

Eigenvector	Band 4	Band 6	Band 7	Band 9
PC1	−0.381390	−0.520636	−0.569137	−0.509473
PC2	−0.888812	−0.020484	0.346498	0.299219
PC3	−0.249450	0.832986	−0.475556	−0.133252
PC4	0.048261	−0.186154	−0.574342	0.795706

Table 5. Eigenvalues of bands 1,4,6,7.

Eigenvector	Band 1	Band 4	Band 6	Band 7
PC1	−0.381390	−0.542373	−0.512020	−0.550961
PC2	−0.912721	0.232838	0.066471	0.329104
PC3	0.100930	−0.598410	−0.251286	0.754038
PC4	0.129014	0.541778	−0.818702	0.139855

the third component in Table 6 were used to reveal Iron oxide (Figure 8), argillic alteration (Figure 9), phyllic alteration (Figure 10) and propylitic alteration (Figure 11) respectively.

2.2.3. Least Squares Regression Fit

To reveal the argillic, phyllic and propylitic alterations, Ls-fit method was applied on all SWIR bands of images obtained from ASTER and the bands of this zone were considered as input bands. Since Kaolinite shows the highest absorb rate in ASTER band 6 (band 3 of SWIR zone), this band was selected as the modeling band. In the resulting figure, the dark pixels represent the argillic alteration and by reversing the numerical values of pixels, bright areas exhibit the argillic alteration (Figure 12). Since chlorite and epidote show the highest absorption in ASTER band 8 (band 5 of SWIR zone) this band was selected as the modeling band. In the resulting figure, the dark pixels represent the propylitic alteration, and by reversing the numerical values of pixels, bright areas exhibit the propylitic alteration (Figure 13). Since iron oxide has the highest reflection in ASTER band 2, to reveal the Iron oxide alteration, bands 3,2,1,4 of ASTER satellite images were used as input bands and band 2 was used as the modeling band, in the resulting image, bright pixels represent iron oxide alteration (Figure 14).

Table 6. Eigenvalues of bands 2,5,8,9.

Eigenvector	Band 2	Band 5	Band 8	Band 9
PC1	0.461782	03482501	0.563748	0.485941
PC2	0.873761	−0.106231	−0.335009	−0.336193
PC3	0.136813	−0.840964	0.511466	0.111640
PC4	0.067686	−0.220650	−0.555301	0.798982
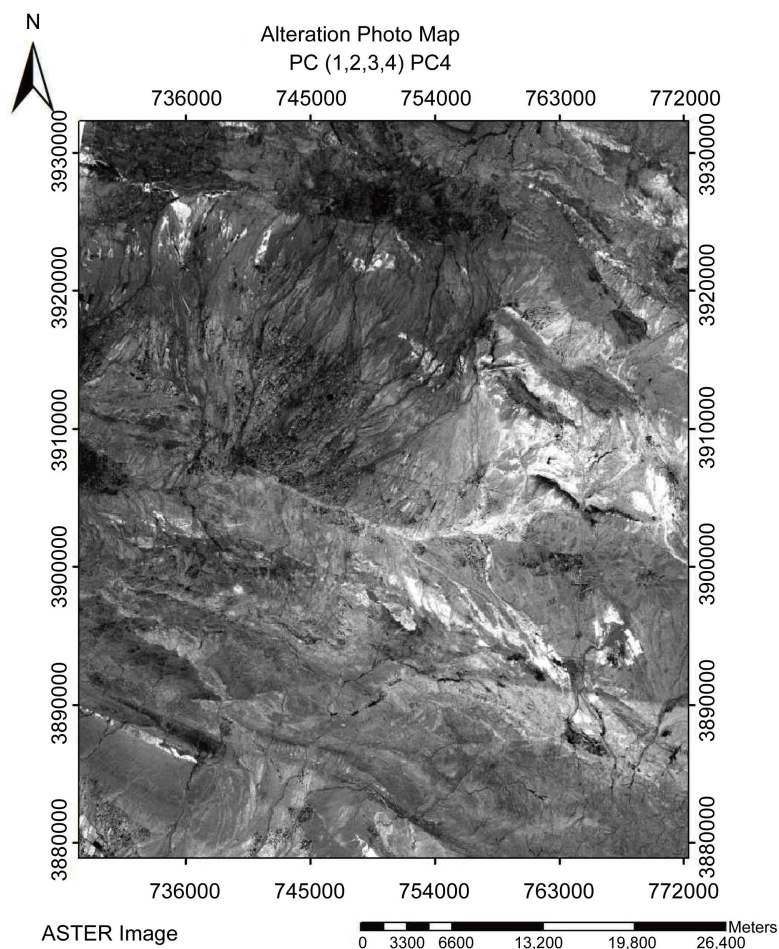
Figure 8. Bright pixels are indicative of iron oxide.

2.2.4. Spectral Angle Mapper (SAM)

In this section, the spectral behaviors of minerals were used to identify different alterations. Kaolinite, dickite, montmorillonite and halloysite were used to identify argillic alteration, muscovite, illite and pyrite were used to reveal phyllic alteration, chlorite and epidote were used for propylitic alteration detection and jarosite, hematite and goethite were used to display iron oxide alteration. Spectral behaviors of all these minerals were checked against USGS Spectral library [5] and it was observed that all the index minerals of each alteration overlap. Figure 15 shows the final alteration map produced by this method.
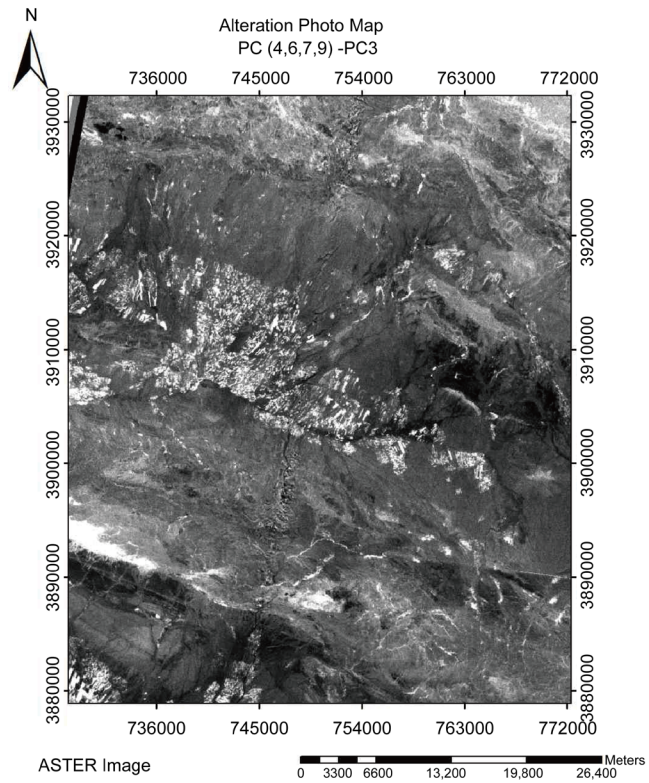
Figure 9. Bright pixels are indicative of argillic alteration.
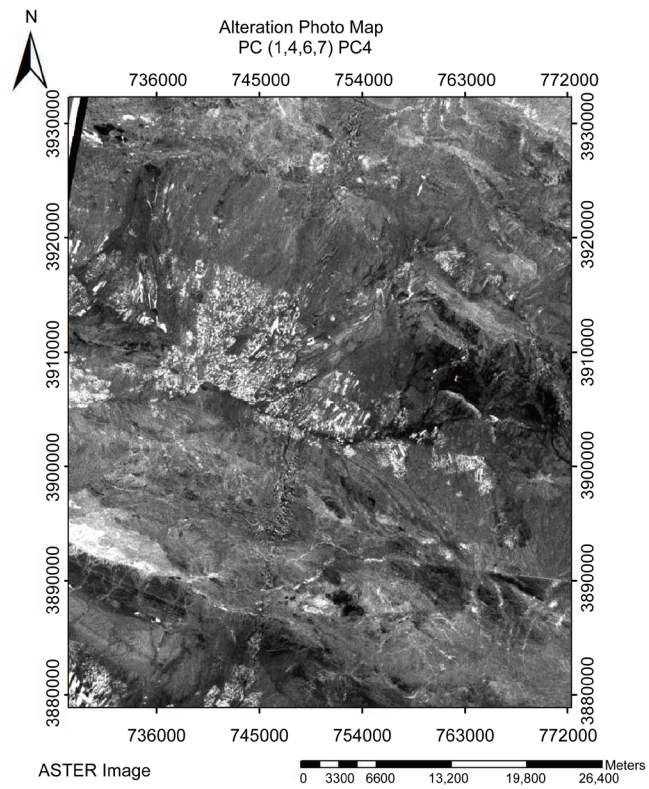
Figure10. Bright pixels are indicative of phyllic alteration.

Scientific Research Publishing
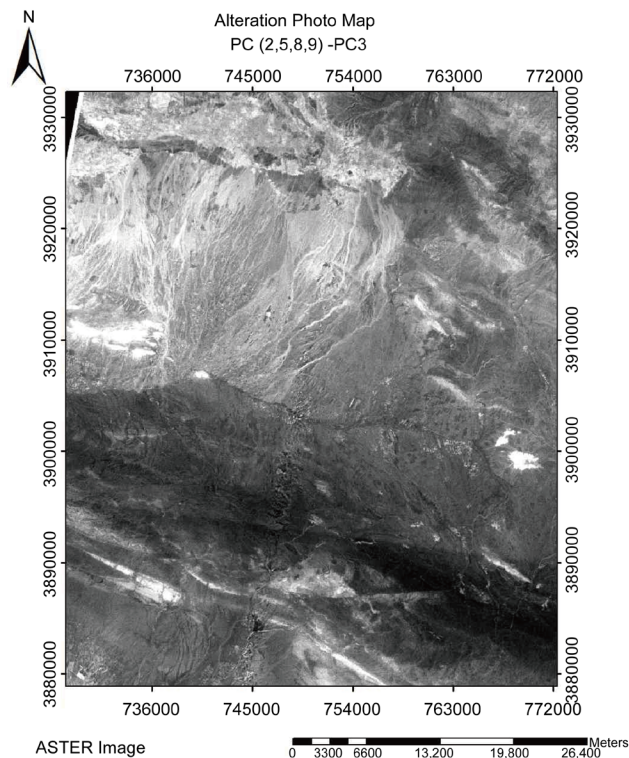
Figure 11. Bright pixels are indicative of propylitic alteration.
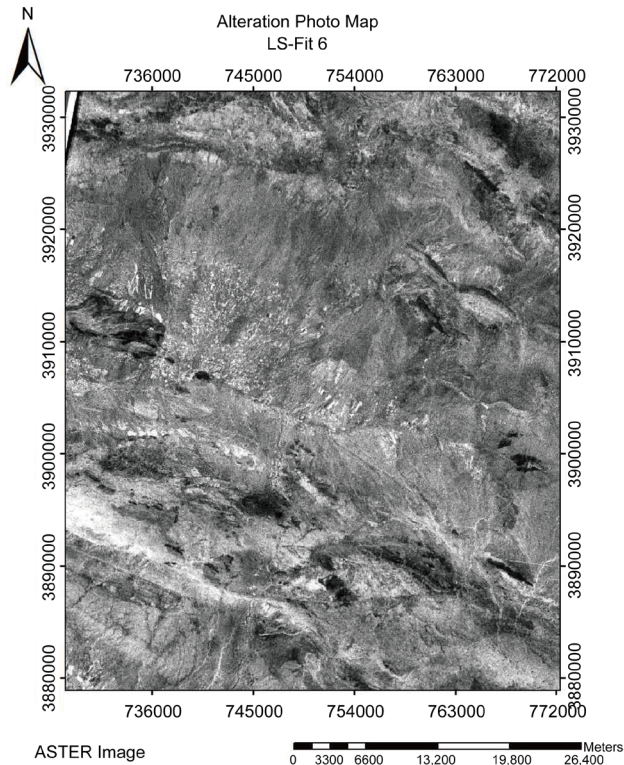
Figure 12. Bright pixels are indicative of argillic and phyllic alteration.
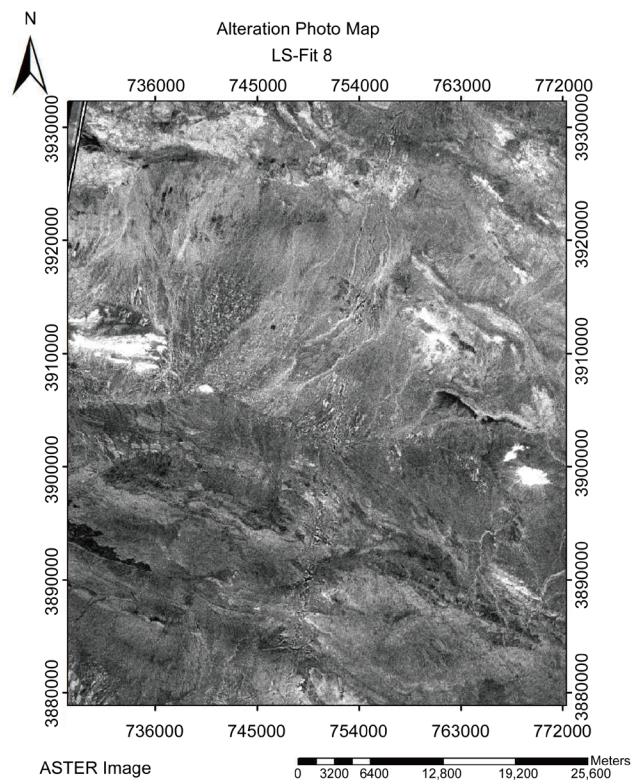
Figure 13. Bright pixels are indicative of propylitic alteration.
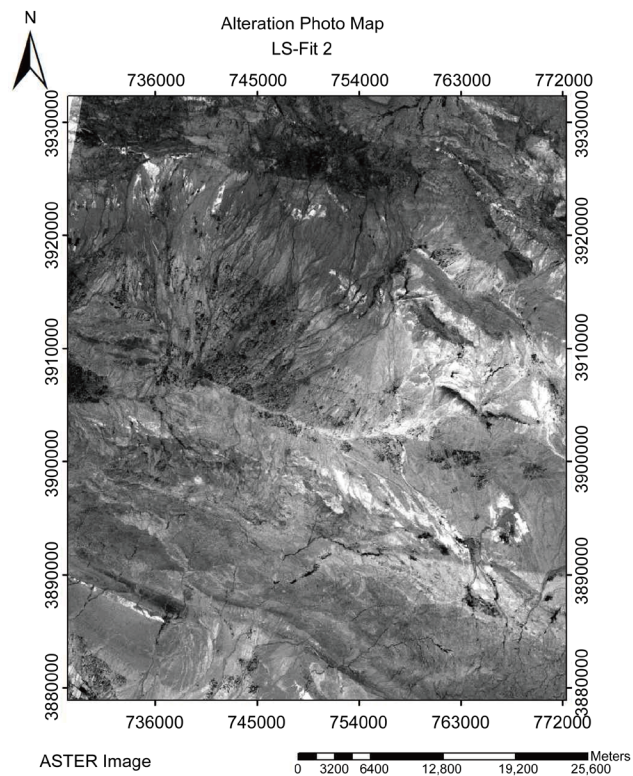
Figure 14. Bright pixels are indicative of iron oxide.
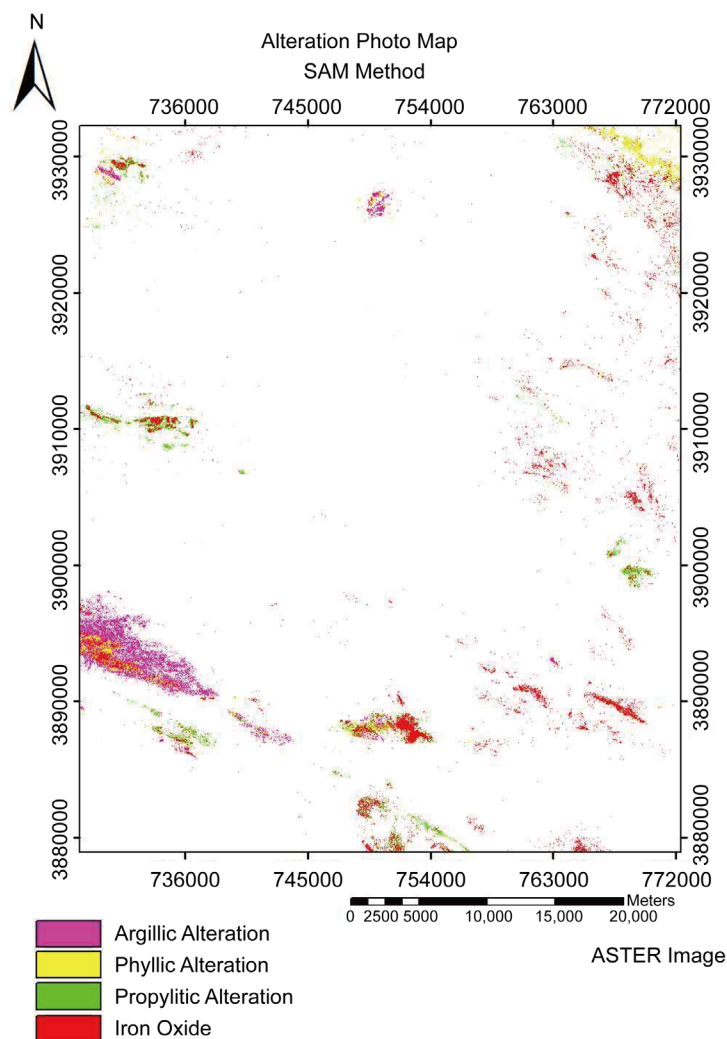
Figure 15. Study area alteration map using SAM method.

2.3. Final Map of Alterations in Study Area

Due to higher number of bands and higher resolution, Aster images can reveal and detect alteration with higher accuracy in comparison to that of OLI's. However, the ability of OLI's images to reveal topographic features cannot be ignored. Figure 16 shows the final map of alterations in the study area which is the result of the integration of all methods.

3. Tectonic

By considering the Doruneh (Kavir bozorg) fault which is in a 1 to 2 Km vicinity of the study area, there is no doubt that shear movements must be considered carefully when studying the area's tectonic. Doruneh fault (velman 1966) or kavir borzog fault (Stocklin 1973) is about 700 km long, extending from Naeen to Doruneh with a NE-SW trend, and from Doruneh region, it curves to the south with an east-west trend, and continues to the Afghanistan border. It seems that Doruneh fault is the continuation of
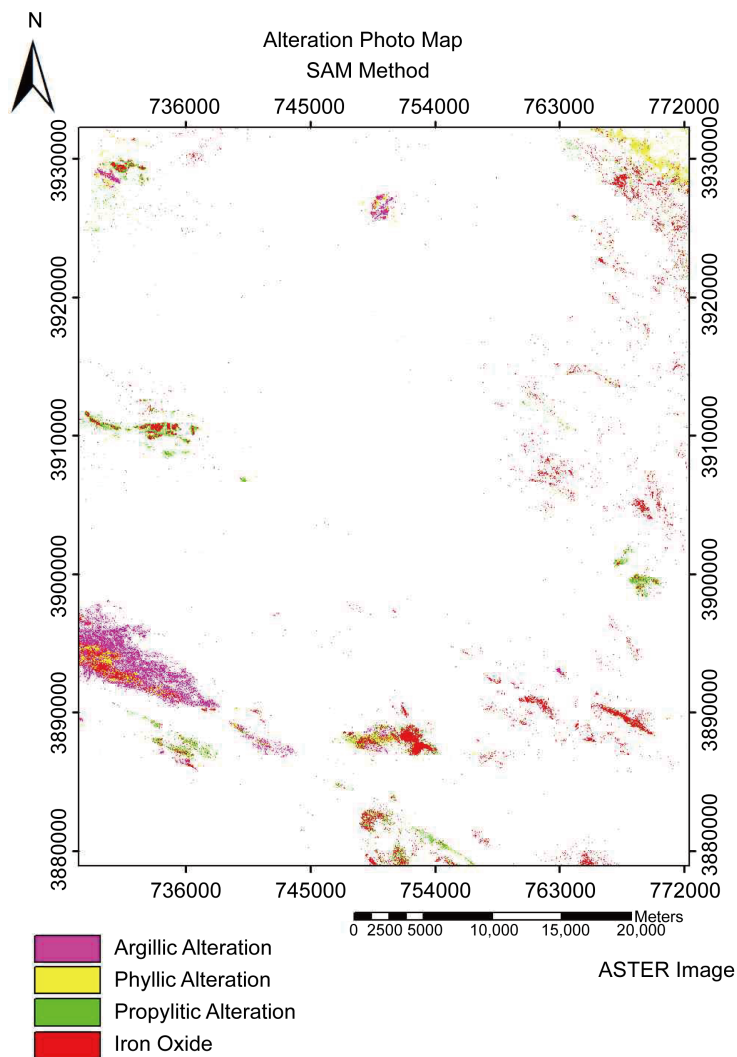
Figure 16. Alteration map derived from the combination of all methods.

Afghanistan's Herat fault. Since the displacement of Doruneh and Herat Fault is about 100 km, it seems that the levorotatory movement of Harirud fault has caused the displacement and separation between these two faults [6].

Considering the diversion of seasonal rivers to the east in the area of the study, it seems that the north block of Doruneh fault has moved to the west, which in terms proves the levorotatory movement. Studying the Slikenside on the border of Andesite porphyry and conglomerates shows that this is a Sinistral fault with the fault plane dip to the south. Since Doruneh fault's last movement was a strike slip movement, the Riedel model can explain the area (**Figure 17**). T fractures in Riedel model are the best place for ore-bearing siliceous solutions intrusion. This phenomenon is confirmed by field observation and sampling, in the way that most of the ore-bearing siliceous veins are extended between 45 to 60 degrees [7].

Overall, two general trends can be considered for the fractures in the area, the first main trend is the NW-SE trend which is aligned with Doruneh faults, the second trend
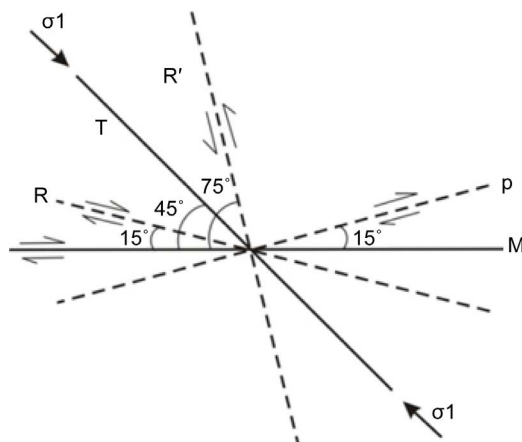
Figure 17. Explanation of fractures in the area resultant from strike-slip fault using Riedle's model.

is almost perpendicular to the first one and most of the ore-bearing siliceous veins form an acute angle with this trend. The trends of these faults have caused many fractures in the area especially in harder units such as Andesite porphyry and granites [8].

To justify the fractures in the area, it can be noted that Porphyry Andesite and granite are very hard units and due to shear forces caused by Doruneh's fault movement, they are extremely tectonized, to the extent that some portions of the lower units can be seen in form of sheets in this unit.

Due to tectonic activities in the area, siliceous veins are not traceable and can only partially be seen. Also in some areas outcrop of porphyry andesite, basalt and agglomerate are seen as intertwined (Figure 18).

4. Geochemistry

4.1. ICP-OES Analysis Results

10 samples were taken from different parts of mineralization in the FATH-ABAD area. These samples were sent to the laboratory for multi-element analysis using ICP-OES method. Results of the analysis are shown in Table 7.

According to the table, samples FA04, FA09, FA12, FA14, FA21, FA22, FA29 were taken from segmented siliceous veins hosted in andesite, latite and conglomerate rocks. Sample FA02 was taken from agglomerate block hosted in andesite and samples FA27 and FA30 were taken from polygenetic conglomerates, according to the analysis results in the above table, copper grades were significant in samples FA12, FA14, FA27, FA29 and FA 30. It should be noted that Sample FA29 was taken from the western end of the area where two siliceous veins intersect. In terms of topography and size of the silica, the point of intersection of siliceous veins is suitable for digging trenches.

4.2. Investigating Alterations in the Study Area

In general, the study area is mostly non-altered and iron oxide alteration is sporadically visible in polygenetic conglomerate only where faulting has occurred.

Figure 18. From left to right, Agglomerate, Basalt, Porphyry Andesite.

Table 7. ICP-OES analysis results.

Element	Ag	As	Cu	Fe	Mg	Mn	XX	YY
Unit	ppm	ppm	ppm	ppm	ppm	ppm		
FA02	0.28	3.3	1064	54,713	18,067	590	756,177	3,881,524
FA04	0.35	2.2	7417	25,591	5304	910	755,635	3,881,872
FA09	0.23	4.9	8869	10,113	434	52	756,974	3,881,074
FA12	0.32	17	31740	53,029	1246	130	757,062	3,880,525
FA14	0.44	8.2	12574	18,815	557	1005	757,697	3,880,406
FA21	0.26	5.3	4202	14,426	514	621	758,744	3,879,975
FA22	0.28	10.6	5445	11,394	615	266	759,060	3,880,151
FA27	4.1	3.5	35463	59,104	18,651	822	755,891	3,881,548
FA29	0.34	8.6	17560	27,226	1698	570	755,439	3,881,922
FA30	1.6	4.5	21,996	47,796	23,742	1231	756,233	3,881,236

In the eastern part of the region, partially altered latite-andesites (argillic-chlorite alteration) are evident; these alterations are also traceable in satellite images. Silicification is limited in the area, which is particularly seen in eastern parts and in some cases it is accompanied by black tourmaline veinlets.

Ultimately, it can be noted that the studied area has been affected by ore-bearing siliceous solutions resulting in formation of siliceous veins and veinlets (in many cases ore bearing) in the entire sedimentary-volcanic unit, veins up to 1.5 m thick are evident in the area. Most of these siliceous veins are hosted in volcanic rocks (Latite-andesite to porphyry andesite). Volcanic units are brittle, the pressure from Doruneh fault has caused the T fracture in the Riedel model to open and Silicic fluids has filled these fractures, hence the accumulation of siliceous veins in volcanic units. Siliceous veins and veinlets are rarely seen in the southern sedimentary units of the area (Due to the flexibility of the marl, shale and sandstones outcrops).

5. Lithogeochemical Investigation

Regional exploration is considered among infrastructural explorations which are aimed

to identify possible mineralization in a relatively vast area, eliminate the sterile regions and discover relation (relevance) between desired regions. In other words, the scope of such explorations is to identify regions where in order to explore mineral deposits, detailed explorations must be conducted. Geochemical mapping in regional scale is one of the principal fundaments of explorations in this scale, where perhaps the most significant results from analysis of geochemical data is separation of various anomalous communities (possible, probable, definite) from each other and determining context for each element in the explored area.

5.1. Sampling Network Design

Optimum design of the sampling network is done based on the center of gravity of streams with varying degrees. **Figure 19** shows the stream samples map.

5.2. Processing Raw Data and Out of Range Values Correction

The Dorffel method was used to correct out of range values. If the mean ($\overline{x}$) and stan-
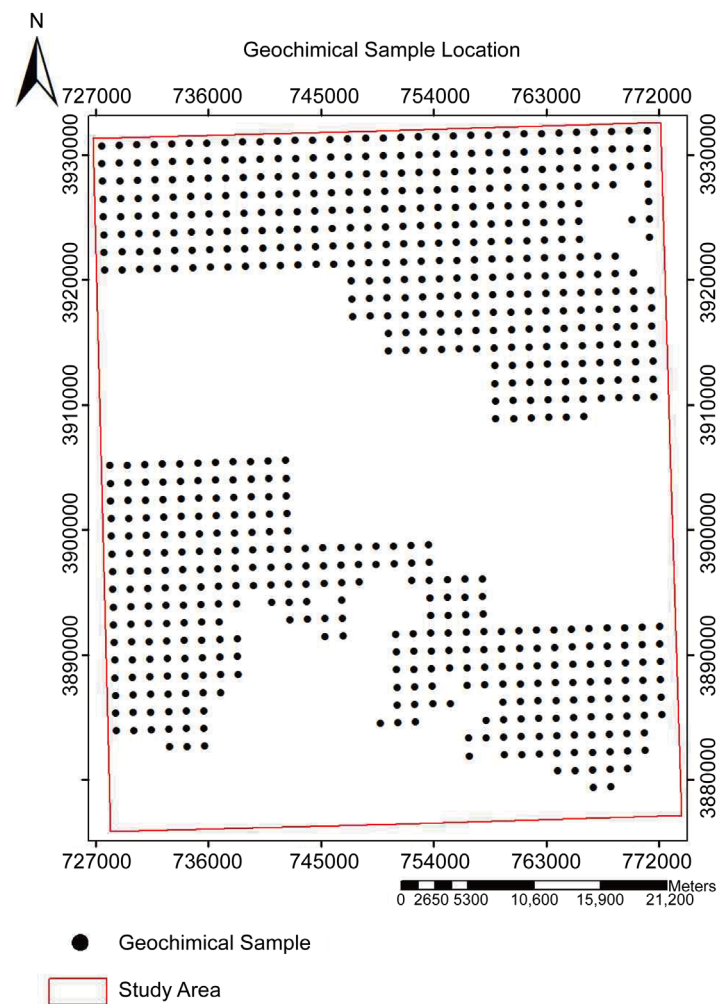
Figure 19. Sampling network design.

dard deviation of data's (s) satisfy the below equation without considering the largest values of data (xA), the result is an out of range value. In the below equation "g" is considered the out of range value threshold [9].

$$XA \geq \overline{x} + s.g$$

First, to calculate the statistical parameters of elements, the raw data of elements was inputted into SPSS software, initial statistical values were calculated and each element's histogram was drawn.

In this stage, the value of Mean, Median, Mode, Standard deviation, Variance, Skewness, Kurtosis, Range, Minimum and maximum values of data were calculated and shown in Table 8.

According to the Table 8 the difference between mean and the median values of elements is due to unbalanced distribution of these variables. The value of the coefficient variation (CV %) represents the variation range of that element. In this project the highest coefficient of variation belongs to Ar and the lowest variation belongs to Mo. After As, Pb has the highest coefficient variation factor, where Mo shows the lowest variance values, Pb and Zn show the highest variance values which can be considered a sign of the concentration dispersion of these elements in the study area. In a normal distribution function, Skewness equals zero and the higher Skewness gets, the more the Statistical population deviates from a normal distribution. Furthermore, the high value of skewness in a geochemical distribution function shows the probability of mineralization or an anomalous existence of that element. Considering the skewness values of data, as shows the highest positive value of skewness whereas Mo shows the lowest positive value of skewness.

5.2.1. Bivariate Statistical Analysis

In order to produce a correlation matrix, raw data was processed in an SPSS software

Table 8. Statistical parameters of studied variables (raw data).

Parameter	Au (ppm)	As (ppm)	Cu (ppm)	Mo (ppm)	Pb (ppm)	Zn (ppm)
Mean	1.11	10.25	31.45	0.82	21.30	78.34
Median	1.08	8.93	27.84	0.8	16.61	67.84
Mode	1	9	24	1	4	56
Std. Deviation	0.567	11.537	13.309	0.564	24.077	35.037
Variance	0.322	133.107	177.117	0.319	579.720	1227.575
Skewness	3.479	14.425	2.959	0.828	6.499	2.954
Kurtosis	22.676	288.515	14.489	4.967	67.601	15.295
Range	6	250	135	4	343	329
Minimum	0	2	10	0	2	38
Maximum	6	252	145	4	345	367
Sum	756	6938	21,290	556	14,422	53,038

environment and the correlation coefficients were calculated and shown in Table 9.

As shown in Table 9, the highest positive correlation values are between Pb and Zn (0.795) Pb and Mo (0.468) Zn and Mo (0.459), whereas the highest negative correlation value is between Pb and Au (−0.087).

5.2.3. Multivariate Statistical Analysis
Among different multivariate statistical analysis methods, Cluster analysis was performed in this project, the Cluster analysis result for the study area is shown in Figure 20.

5.3. Final Geochemical Anomaly Map
To draw the studied area anomaly map, the Inverse Distance Weighting (IDW) method was used. Figures 21-26 show the anomaly maps of stream sediments. Given the scale of the study area, cell Dimensions were considered 100 m.

Table 9. The coefficient correlation of elements in streams sediments.

Parameter	As	Cu	Mo	Au	Pb	Zn
As	#	0.019	0.236	0.039	0.241	0.247
Cu		#	−0.042	0.340	0.112	0.144
Mo			#	−0.046	0.468	0.459
Au				#	−0.087	−0.1
Pb					#	0.795
Zn						#
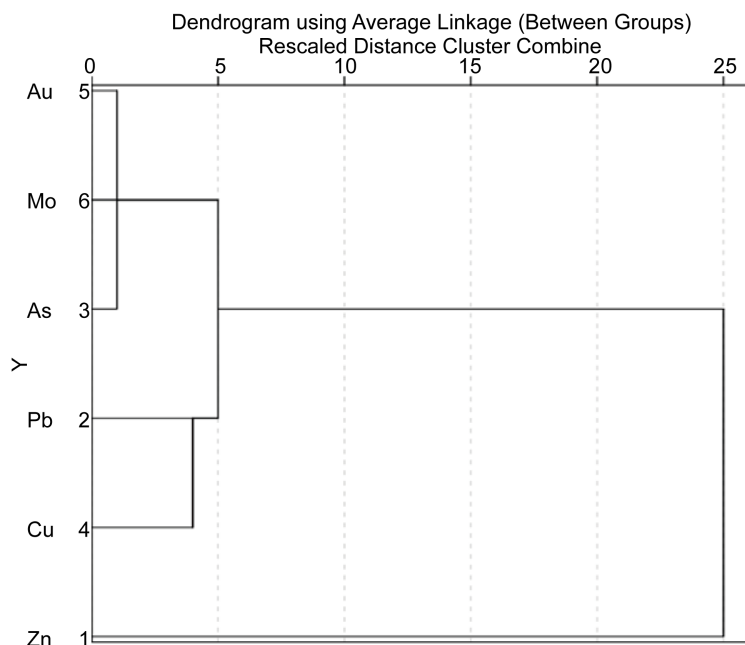
Figure 20. Cluster analysis dendrogram.
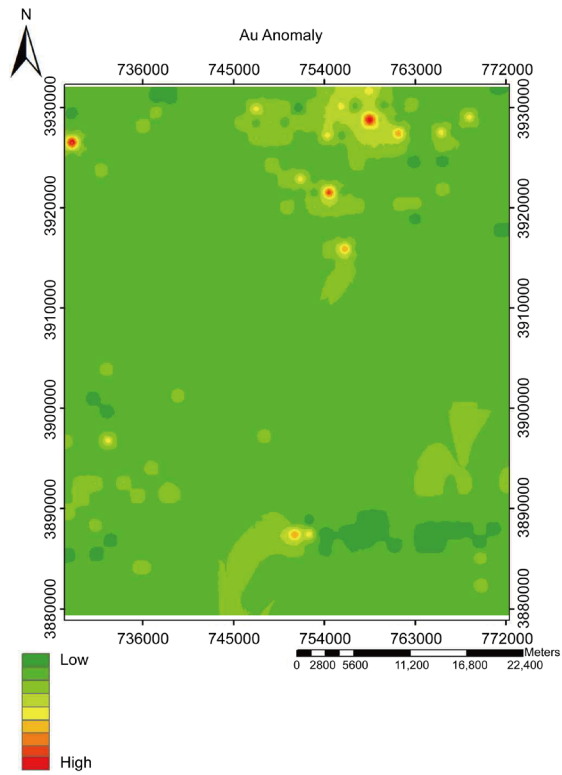
Figure 21. Au anomaly map.
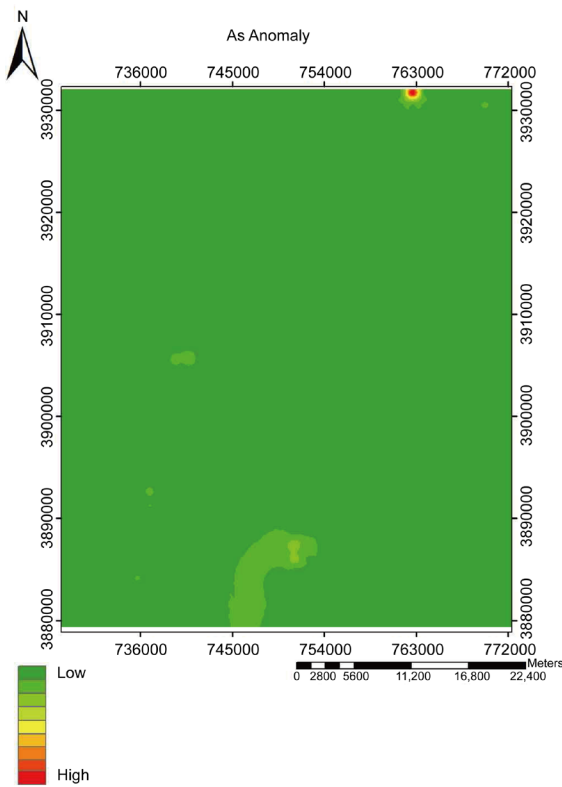
Figure 22. As anomaly map.
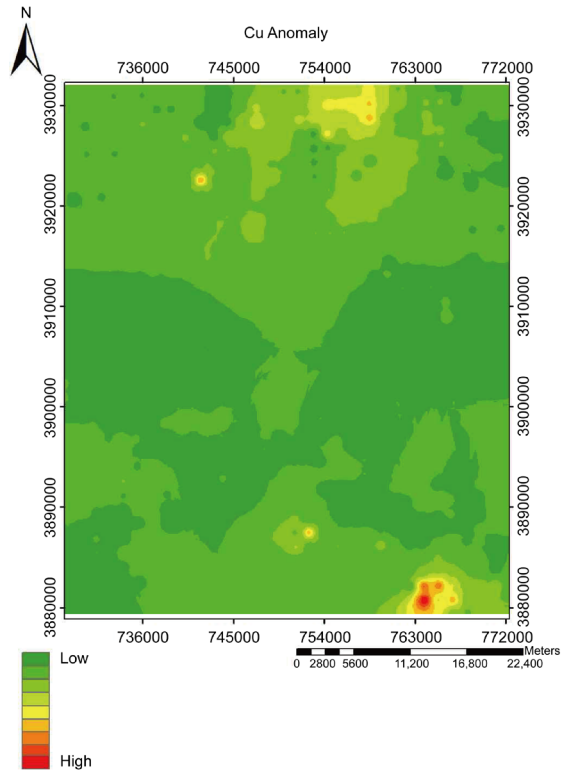
Figure 23. Cu anomaly map.
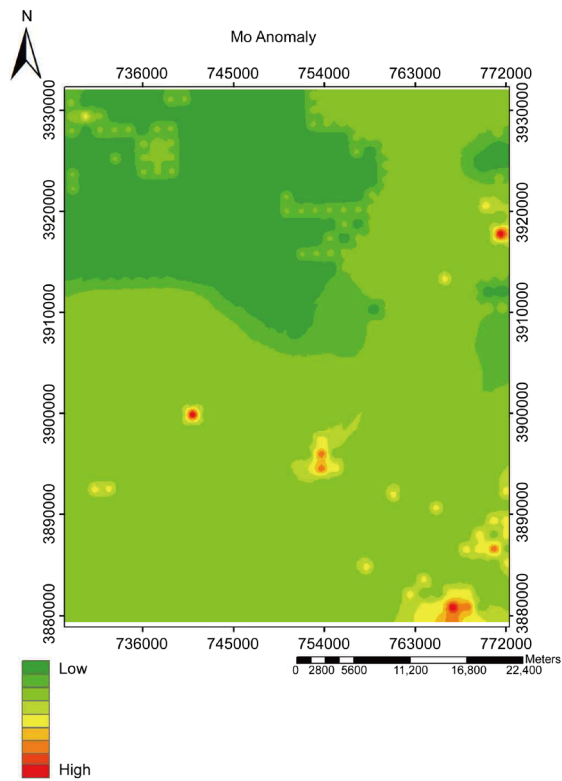
Figure 24. Mo anomaly map.
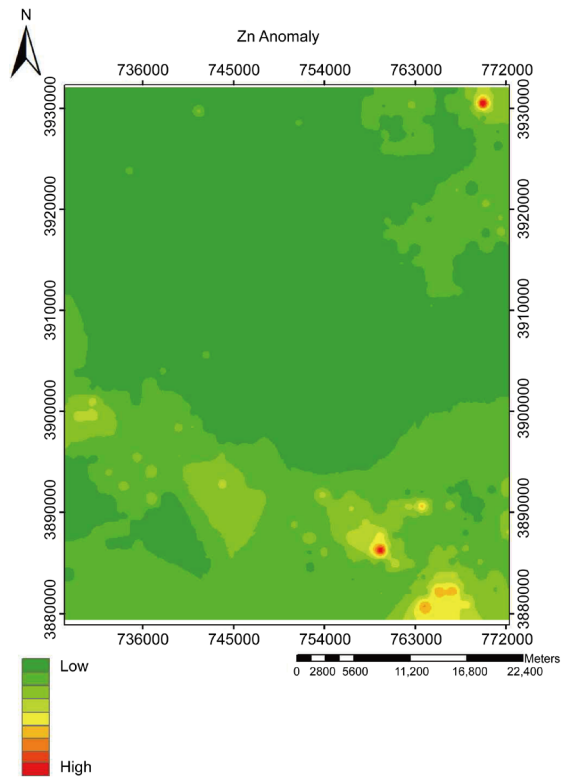
Figure 25. Zn anomaly map.
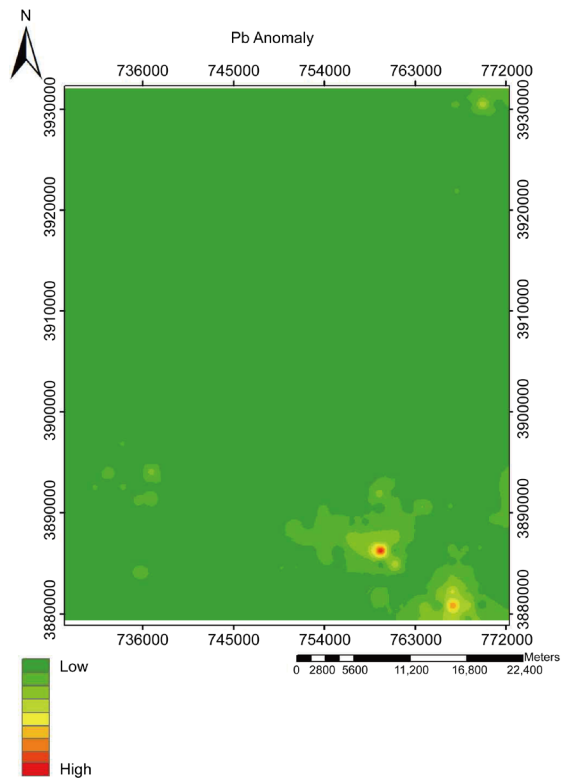
Figure 26. Pb anomaly map.

According to the anomalies map it is clear that the elements Cu, Pb, Zn and Mo show a good overlapping in the southern part of the map, so the possibility of mineralization in the overlapped area is expected.

6. Discussion

Considering the existence of oxide mineralization on the surface and outcrops of copper oxide mineralization in the fault zone, the relationship between geological structures and mineralization was carefully studied. The studies show that at least 4 types of Cu mineralization are present in Fath-Abad exploration area. The first type is oxide mineralization along with polygenetic conglomerates, the second is oxide mineralization hosted in andesite and latite-andesite rocks in the eastern part of the. The third, type is sulfide-oxide mineralization in silica. The fourth, type is sulfide- oxide mineralization in agglomerate spots accompanied with rounded silica bits. This mineralization is visible in porphyry andesite units where faulting has occurred.

Oxide mineralization in polygenetic conglomerate: Open space filling mineralization has occurred in polygenetic conglomerates. This form of mineralization is mainly seen in 2 areas but minor mineralization is available in some places. One of the main areas of mineralization is situated in the western part of the study area where a main trench is being dug. Mineralization in this area is 20 m long (N-S trend) and 10 m wide (E-W trend).

Along the fault between the porphyry andesite unit and conglomerates, segmented mineralization with 4 * 5 m in dimension is visible. These mineralizations are characterized by significant presence of oxide minerals such as malachite. Moreover the Superficial and mushroom shaped spreading of mineralization, existence of iron oxides and red colored rock units are other features of mineralization in this part of the study area. In this part of the area, mineralization stretches about 200 m, but it occurs in a sporadic pattern. In many places there are no clear relation between mineralization and faults. The red colored Conglomerate unit does not extend to the east but it stretches to the west. Due to an abundance of faulting activities and coverage with alluvial terraces, the conglomerate is only visible in some places (Figure 27).

It seems that oxide mineralization is accompanied by thin sulfide mineralization (perhaps as thin as a few centimeters) in depth.

Oxide mineralization hosted in andesite and latite-andesite rocks: Continuing to the east along the mineralization zone, a substantial oxide mineralization has occurred in Latite-andesite units. In this part, Cu oxide mineralization is formed in fractures and mostly consists of malachite. Trenches in the area confirm the existence of Cu oxide mineralization, mineralization is segmented and each segment is 6 m wide, approximately 30 m in length and 2 to 3 m in depth (Figure 28).

Sulfide-oxide copper mineralization in silica veins: Milky colored silica veins are evident in many parts of the area, these veins are usually 20 to 30 cm thick, however, some veins are 1 m thick and can reach up to 20 m in length. Severe faulting has caused the veins to appear as segmented. These veins are usually milky colored and an abun

Figure 27. Oxide mineralization associated with the fault and presence of iron oxides in hosting polygenetic conglomerate rock.

Figure 28. Copper oxide mineralization evident in parts extracted from trenches.

dance of sulfide minerals such as Chalcopyrite is considered a predominant feature of this type of mineralization. Due to the resistance of quartz to weathering, sulfide minerals have largely remained intact. However, where weathering has occurred, most sulfide minerals have altered to oxides such as malachite (**Figure 29**).

In this section, silica veinlets with 0.5 to 2 cm thickness have formed inside the host rock. In some cases, these veinlets have a dogtooth texture and they have probably been replaced in tensile joints during strike slip faulting processes

Sulfide-oxide mineralization in agglomerate: Agglomerate blocks with semi-rounded fragments of silica are found in porphyry andesite unit with border fault, where the mineralization generally consists of chalcopyrite and malachite. These mineralizations generally occur in 5 * 5 m areas. However, their occurrences are very limited (**Figure 30**).

After acquiring, preparing and evaluating different layers of data, these data were

Figure 29. Oxide mineralization associated with the fault and presence of iron oxides in hosting polygenetic conglomerate rock.

Figure 30. Agglomerate blocks with semi-rounded fragments of silica are found in porphyry andesite.

compiled together using the index overlay method to introduce areas suitable for mineralization. In this method pixels of different data layers, each of which has its own value, are overlapped and ultimately pixels with the highest value are displayed. This way, areas in all layers of data ranging from geological, geochemical and remote sensing that have the highest possibility of mineralization are displayed. **Figure 31** shows the anomaly map resulting from overlapping different data layers using the Index overlay GIS modeling.

7. Conclusions

Up to this exploration, geological and geochemical studies have been conducted on Fath-Abad area and by incorporating the results, it is evident that metallic mineralization is significant in southern and southwestern regions of the area. In order to com-
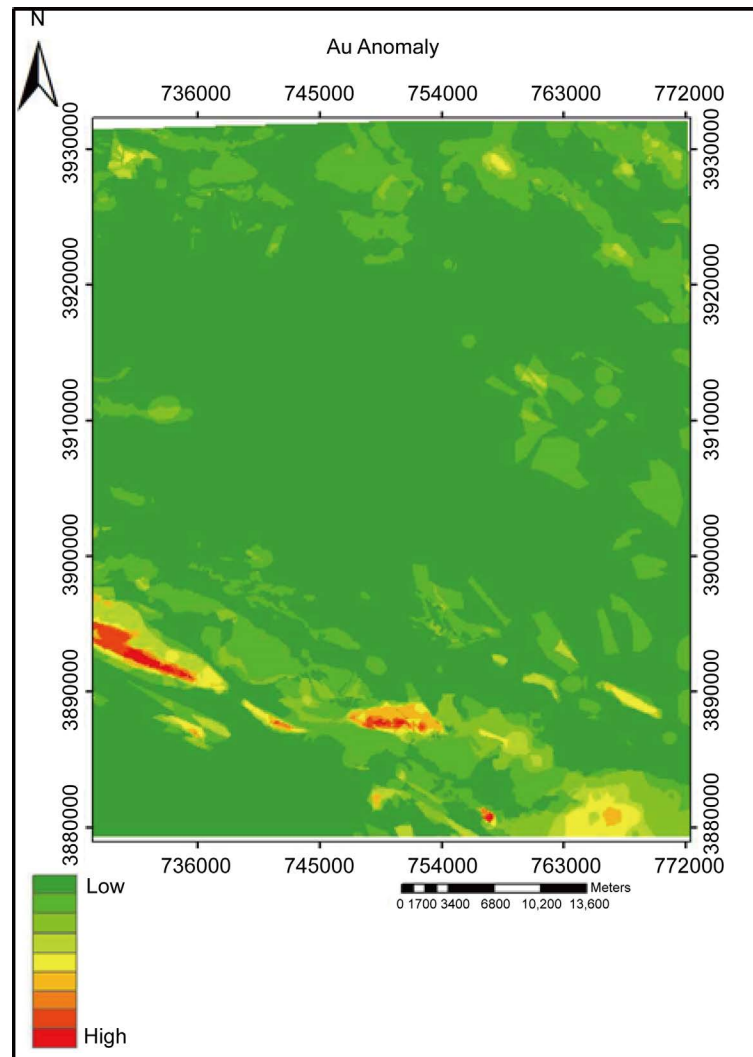
Figure 31. Anomaly map resultant of integrating data layers using index overlay method.

pare mineralization in study area with standard universal mineralization models, the most prominent aspects of the area such as mineralization, host rock, alteration, rocks age range, tectonic position, structural controls and geochemical characteristics are as follows: 1. Mineralization: Chalcopyrite occurs in siliceous veins and veinlets as interstitial space-filling minerals whereas pyrite mostly exists within the rocks; 2. Host rock: mega porphyry Andesite, conglomerate and sedimentary units; 3. Alteration: low argillic alteration has occurred in intrusive bodies and alongside the fertile faults of the area silicic alteration has occurred; 4. Geological age range: Eocene-Oligocene; 5. Tectonic position: the area is situated near active volcanic centers and on the Doruneh basement fault; 6. Structural controls: mineralization has occurred predominantly along steep faults; 7. Geochemical features: anomaly of As, Ag, Sb, Bi, Pb, Mo, W is present in the area, and surface distribution of these anomalies conforms to the faults present in the area.

Economic geology studies on the area was conducted with the goal of integrating various data such as ASTER-OLI satellite images, however, satellite data with higher ground resolution can reveal more abnormalities. Therefore, it is suggested that hyperspectral satellite image processing should be placed on the future studies' agenda.

Also, since the presence of Cu-Au mineralization is confirmed, fluid inclusion studies and Stable Isotope analysis are recommended with the aim of studying S Isotopes present in sulfide minerals.

References

[1] Bijan K.M., *et al.* (2009)Khorasan Razavi Geological Report, Geological Survey and Mineral Exploration of Iran, Report No. 376.

[2] Agha-Nabati, S.A. (2012) Geology of Iran.

[3] Porkermani, M. and Arian, M. (1998) Iran's Seismicity 76.

[4] Loughlint, W.P. (1991) Principal Component Analysis for Alteration Mapping. American Society for Photogrammetry and Remote Sensing, Vol. 57, 1163-1169.

[5] Clark, R.N., Swayze, G.A., Wise, R., Livo, K.E., Hoefen, T.M., Kokaly, R.F. and Sutley, S.J. (2007) USGS Digital Spectral Library Splib06a. U.S. Geological Survey, Data Series 231.

[6] Stöcklin, J. and Setudehnia, A. (1971) Stratigraphic Lexicon of Iran: Central, North and East Iran. Geological Survey of Iran, Report No. 16, 372 p.

[7] Price, N.J. and Cosgrove, J.W. (1990) Analysis of Geological Structures. p. 144.

[8] Saadat, S. (2006) The Study of Potential Mineralization and Exploration Priorities in Eastern Region of Iran, Geological Survey and Mineral Exploration of Iran.

[9] Jozani Kohan, G. (2015) Principals of Instrumental Analysis of Minerals. *Journal of Engineering Geology*, 10-34.